ChemPubSoc Europe

DOI: 10.1002/chem.201404669

CHEMISTRY
A European Journal
Full Paper

Photochemistry

Substituent and Solvent Effects on the Excited State Deactivation Channels in Anils and Boranils

Jacek Dobkowski,[a] Paweł Wnuk,[a, b] Joanna Buczyńska,[a] Maria Pszona,[a] Grażyna Orzanowska,[a] Denis Frath,[c] Gilles Ulrich,[c] Julien Massue,[c] Sandra Mosquera-Vázquez,[d] Eric Vauthey,*[d] Czesław Radzewicz,[b] Raymond Ziessel,*[c] and Jacek Waluk*[a, e]

Abstract: Differently substituted anils (Schiff bases) and their boranil counterparts lacking the proton-transfer functionality have been studied using stationary and femtosecond time-resolved absorption, fluorescence, and IR techniques, combined with quantum mechanical modelling. Dual fluorescence observed in anils was attributed to excited state intramolecular proton transfer. The rate of this process varies upon changing solvent polarity. In the nitro-substituted anil, proton translocation is accompanied by intramolecular electron transfer coupled with twisting of the nitrophenyl group. The same type of structure is responsible for the emission of the corresponding boranil. A general model was proposed to explain different photophysical responses to different substitution patterns in anils and boranils. It is based on the analysis of changes in the lengths of CN and CC bonds linking the phenyl moieties. The model allows predicting the contributions of different channels that involve torsional dynamics to excited state depopulation.

Introduction

Understanding of the elementary steps of ultrafast photoinduced phenomena, such as electron or proton/hydrogen transfer or conformational changes is the prerequisite for comprehensive description of basic natural processes: photosynthesis and vision. It is also crucial for applications in numerous areas: materials science, optoelectronics, information storage, design of sensors, biology, medicine, and environmental protection. A particular case, challenging both for experimentalists and theoreticians, arises when more than one channel participates in excited-state deactivation, either in a competing or cooperative way. The best known examples include proton-coupled electron transfer[1–8] and excited state electron transfer accompanied by structural changes.[9–13] It has been recently proposed that also photoinduced proton transfer can be coupled to a conformational change, involving mutual twisting of proton donor and acceptor moieties.[14]

In this work, we analyse the experimental and theoretical results obtained for a series of anils (aniline-imines) and boranils (Scheme 1). These compounds can formally be derived from *N*-salicylideneaniline (SA), the most investigated molecule of the Schiff base family, famous for extremely complex behaviour involving ultrafast excited state intramolecular proton transfer (ESIPT), torsional dynamics, photochromism, thermochromism, and solvatochromism.[15–44] Upon photoexcitation, the enol form of SA undergoes ultrafast intramolecular proton transfer from the hydroxy group to the nitrogen atom. This leads to a *cis*-keto form, which is subsequently converted into a photochromic product (*trans*-keto tautomer).

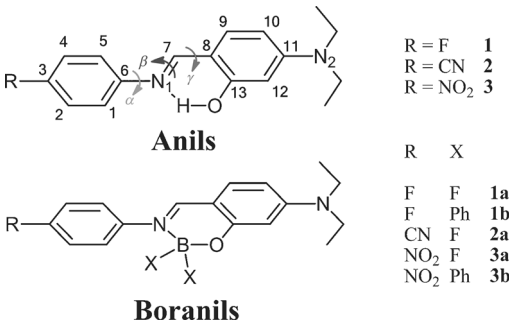

Scheme 1. The investigated anils and boranils.

[a] Dr. J. Dobkowski, Dr. P. Wnuk, Dr. J. Buczyńska, M. Pszona, G. Orzanowska, Prof. J. Waluk
Institute of Physical Chemistry, Polish Academy of Sciences
Kasprzaka 44, 01-224 Warsaw (Poland)
E-mail: waluk@ichf.edu.pl

[b] Dr. P. Wnuk, Prof. C. Radzewicz
Institute of Experimental Physics, Faculty of Physics
University of Warsaw, Hoża 69, 00-681 Warsaw (Poland)

[c] Dr. D. Frath, Dr. G. Ulrich, Dr. J. Massue, Prof. R. Ziessel
Laboratoire de Chimie Organique et Spectroscopies Avancées
UMR7515 au CNRS, École de Chimie
Polymères Matériaux de Strasbourg, 25 rue Becquerel
67087 Strasbourg, Cedex 02 (France)
E-mail: ziessel@unistra.fr

[d] Dr. S. Mosquera-Vázquez, Prof. E. Vauthey
Department of Physical Chemistry, University of Geneva
30 quai Ernest-Ansermet, 1211 Geneva 4 (Switzerland)
E-mail: eric.vauthey@unige.ch

[e] Prof. J. Waluk
Faculty of Mathematics and Natural Sciences
College of Science, Cardinal Stefan Wyszyński University
Dewajtis 5, 01-815 Warsaw (Poland)

Supporting information for this article is available on the WWW under http://dx.doi.org/10.1002/chem.201404669.

However, both experiment and theory suggest that several other channels may be competing with or following the proton transfer (Scheme 2). These include twisting about CN or CC bonds, $^1\pi\pi^* \rightarrow {}^1n\pi^*$ internal conversion, and singlet–triplet intersystem crossing. Using boranils, compounds devoid of proton-transfer functionality, allows to focus on the role of torsional dynamics not competing with tautomerization, since the possibility of twisting about the C6N1 and C7N1 bonds is retained in these molecules. Moreover, functionalizing SA with electron-donating and -accepting groups allows the study of the role of electronic structure on the kinetics and thermodynamics of both proton transfer and rotational isomerism. Finally, substitution stabilizes the $\pi\pi^*$ versus $n\pi^*$ states, reducing the possible contribution from the internal conversion channel. We demonstrate that the ESIPT rate in anils can be controlled by the nature of substituent and by the polarity of the environment. For both anils and boranils, we show the existence of an effective non-radiative excited state depopulation channel which is activated in polar environment.

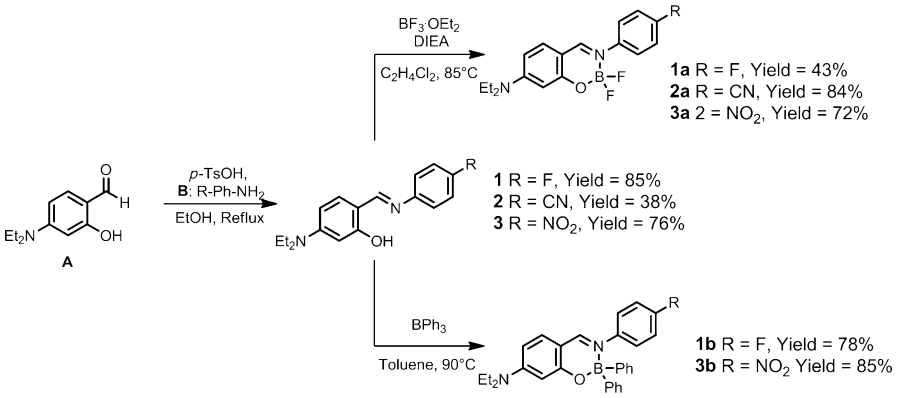

Scheme 3. Synthetic pathways for anils and boranils.

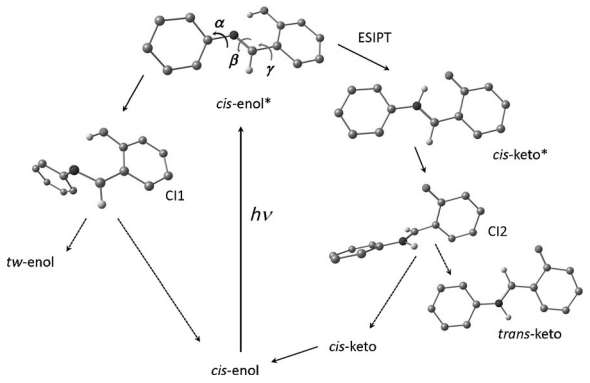

Scheme 2. Possible channels of excited state deactivation in SA. CI1 and CI2 indicate structures corresponding to the region of S_1/S_0 conical intersection.

Results

The synthetic pathway leading to anils[45] and boranils[46,47] is described in Scheme 3. Preparation of the anils **1**–**3** can easily be achieved by treatment of salicylaldehydes A with the appropriate aniline B. This condensation occurs in refluxing ethanol with a catalytic amount of *p*-TsOH. The desired imines precipitate pure out of the reaction mixture and can be purified by filtration with yield from 38 to 85%. Subsequent boron(III) complexation is achieved in 1,2-dichloroethane with $BF_3{\cdot}Et_2O$ under basic conditions to form boranils **1a**–**3a** with yield ranging between 43 and 72%. Boranils **1b** and **3b** are prepared from the BPh_3 precursor in hot toluene with respective yield of 78 and 85%. All these compound have been consistently characterized by ^1H, ^{13}C, ^{11}B NMR, mass spectroscopy and elemental analysis.

Figure 1 shows room temperature electronic absorption and fluorescence spectra of **1**, **1a**, and **1b**, recorded in a nonpolar and a polar solvent, toluene and acetonitrile, respectively.

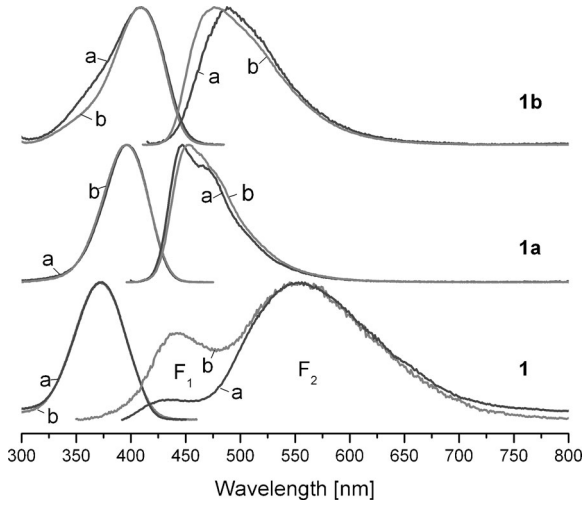

Figure 1. Left: absorption; right: fluorescence of **1**, **1a**, and **1b** in: a) toluene, and b) acetonitrile at 293 K.

The absorption spectra in two solvents are very similar for all three compounds. This claim is also true for the emission profile of **1a** and **1b** in both solvents. In contrast, fluorescence of anil **1** is strikingly different from the emission of boranils **1a** and **1b**: it consists of two bands, of which the higher intensity, low energy one (F_2) is located at similar energies in toluene and acetonitrile. The high energy band (F_1) is barely detectable in toluene, but is clearly observed in a polar environment. The F_1/F_2 intensity ratio is much higher for acetonitrile than for toluene. The total fluorescence quantum yield is quite low (10^{-3} or less, see Table 1); it is about four-times higher in toluene.

The single fluorescence observed for **1a** and **1b** is much more intense than the emission of **1**. It is definitely stronger for toluene than for acetonitrile for **1a** and only slightly so in **1b**. The intensity and lifetime ratios are similar.

Table 1. Spectral and photophysical room temperature characteristics.

	λ_{max} [nm] abs	em	ϕ_{fl}[a]	Decay time [ps] FU[b]	SPC[c]	TA[d]
1						
toluene	372	430/553	0.0011	0.25/61	56 (550)	0.04/57[e]
acetonitrile	372	445/554	0.00025	0.41/45	48 (500, 550)	0.4/40[e]
butyronitrile						0.7/46[e]
1a						
toluene	396	447	0.046		120 (450, 500)	0.6/150
acetonitrile	395	453	0.0085	0.45/20	20 (450)	0.4/25
butyronitrile						0.82/36
1b						
toluene	409	488	0.11		760 (500)	
acetonitrile	409	480	0.07		670 (500)	
2						
toluene	398	460/570	0.0019	0.83/236	220 (570)	0.9/210[e]
cyclohexane				0.49/160		
acetonitrile	398	482/567	0.0018	2.2/160	200 (480)	2.5/150[e]
butyronitrile	399	476/568	0.0016			3.0/175[e]
valeronitrile						2.8/190[e]
THF	400	471/559	0.0017			
2a		461				
toluene	416	468	0.50		1510 (460)	2.7/85/1500
acetonitrile	416	466	0.0083	0.77/17		0.7/6/21
butyronitrile	416	466	0.010			0.4/4/33
THF	411		0.015			0.7/13/90
3		514				
toluene	428	525/680	0.010	1.2/13	260 (525)	8.6/260/$>$3000
acetonitrile	431	514/652	0.0005	0.22/4.2		0.15/0.45/5
butyronitrile	431		0.0068		35 (600)	0.5/1.5/33
3a						
toluene	426	477	0.53		1610	0.3/4.5/2000
acetonitrile	429	494/650	0.0006	0.5/2.6		0.3/5.1
butyronitrile	429	504/630	0.0045		30 (610, 660)	1/2/18
3b						
toluene	440	509	0.61[f]		2730[f]	
acetonitrile	444	518/660	0.0007	0.27/80		

[a] Estimated error: ±20–30% for quantum yields larger than 0.001 and ±50% for lower values. [b] Fluorescence upconversion. [c] Single photon counting; in parentheses, detection wavelength [nm]. [d] Transient absorption. [e] Long-lived component also detected, see Figures S4 and S6 in the Supporting Information. [f] Reference [46].

Because of the difference in the fluorescence patterns in the anil and boranils, the origin of the dual emission of **1** can be readily assigned to the excited state proton transfer, a process responsible for the lower energy emission band F_2. The large increase of the F_1/F_2 intensity ratio in acetonitrile indicates that the reaction barrier is higher in a polar environment, which may be a consequence of a larger excited state dipole moment in the initially excited form. As discussed below, this hypothesis was confirmed by calculations.

The emission spectra of **2** and **2a**, shown in Figure 2, are qualitatively similar to those of **1** and **1a**, but the quantitative differences are significant. Again, a single fluorescence is observed for the boranil derivative **2a**. It is very intense in toluene (quantum yield of 50%), but drops dramatically in acetonitrile, as well as in less polar solvents such as THF and butyronitrile (Table 1). Analogous decrease is observed for the fluorescence decay time. The anil derivative **2** exhibits a dual emission profile in both polar and nonpolar solvents. The F_1/F_2 intensity ratio is strongly solvent-dependent: 0.2 in toluene, 0.6 in THF and butyronitrile, and 0.9 in acetonitrile. This trend is similar to that observed for **1**, but in **2** the F_1 band is definitely more intense with respect to F_2 in each solvent. As was the case for **1**, the dual emission in **2** is assigned to the ESIPT process. The dual emission profile of **2** has been recently reported and interpreted in the same way.[44]

Figure 3 presents the spectra of the nitro derivatives **3**, **3a**, and **3b**. The emission pattern of the anil **3** is quite different from that exhibited by **1** and **2**. A single fluorescence band peaking at 514 nm is observed in toluene solution. In contrast, dual emission is detected in acetonitrile, with the maximum of the dominant, low energy band peaking at 680 nm. A similar behaviour is observed for butyronitrile solution of **3**, but the maximum of F_2 lies at 652 nm, about 30 nm blue-shifted compared to acetonitrile. Such behaviour is different from that of **1** and **2** which exhibit F_2 at similar wavelengths in both polar and nonpolar solvents. The F_1 emission is barely detectable at room temperature in anhydrous acetonitrile and in anhydrous butyronitrile. In acetonitrile its intensity increases with respect to F_2 over a period of several days, which suggests that it may be due to

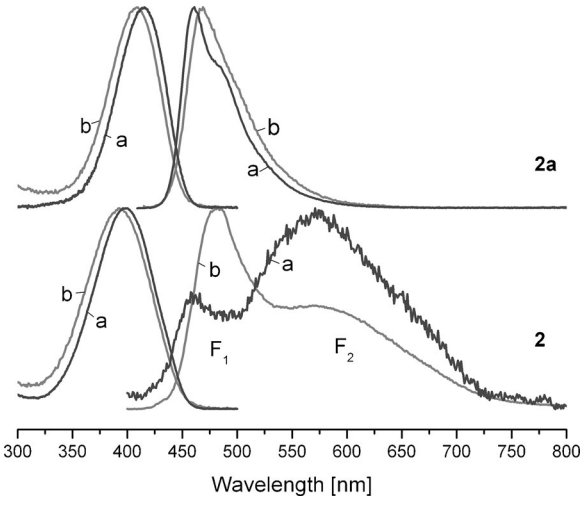

Figure 2. Left: absorption; right: fluorescence of **2** and **2a** in: a) toluene, and b) acetonitrile at 293 K.

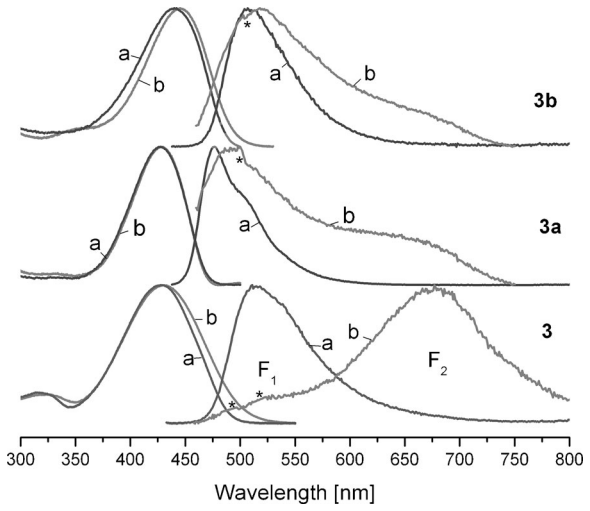

Figure 3. Left: absorption; right: fluorescence of **3**, **3a**, and **3b** in: a) toluene, and b) acetonitrile at 293 K. The asterisks mark artefacts in the emission spectra in acetonitrile due to non-perfect removal of solvent Raman lines.

formation of complexes with water (cf. the section below devoted to the spectra in protic solvents).

The boranils **3a** and **3b** exhibit single emission in toluene, but in acetonitrile a second, low intensity band corresponding to F_2 is observed. Its location is similar to that of F_2 emission of **3**.

In a similar fashion as for **2a**, huge differences in quantum yields and lifetimes are observed for **3a** and **3b** in toluene and acetonitrile. In the latter fluorescence intensity drops by over two orders of magnitude.

The emission behaviour of **3** suggests a different pathway of S_1 deactivation than in **1** and **2**. The observed huge shift of the emission maximum with changing solvent polarity points to a charge transfer character of the excited state. Moreover, contrary to the case of fluoro and cyano derivatives, dual emission is observed for **3a** and **3b**, analogous to that of **3**. One should note, however, very different F_1/F_2 intensity ratios observed for the anil and boranils, suggesting that the photophysical properties are sensitive to the presence of intramolecular hydrogen bonding, which may lead to geometry changes or to different relative positions of low-lying electronic states.

Temperature dependence of the emission

Stationary fluorescence spectra were recorded as a function of temperature in a number of solvents. For toluene, THF, and butyronitrile solutions of **2**, similar changes in the F_1/F_2 intensity ratio are observed (Figure S1 in the Supporting Information): the intensity of both bands increases about five times at lower temperature. Interestingly, the F_1/F_2 ratio initially decreases and then increases upon lowering of temperature; at 294 and 180 K this ratio is practically the same for all three solvents. At lower temperatures in butyronitrile the F_1 fluorescence intensity significantly increases with respect to F_2. At 77 K, phosphorescence is observed: for toluene, its intensity is similar to that of F_1, whereas in butyronitrile it is about three-times weaker.

The temperature dependence of the single fluorescence observed in **2a** (Figure S2 in the Supporting Information) is very different in toluene versus THF and butyronitrile. In toluene, the emission is intense already at room temperature and does not change much as the temperature decreases. On the contrary, in THF and BuCN the emission intensity strongly increases at low temperature. As a result, practically the same fluorescence quantum yield values are determined at 173 K: 0.27 (BuCN), 0.24 (THF), 0.21 (toluene). At 77 K in toluene, no phosphorescence is observed, contrary to the behaviour of **2**.

Very strong temperature dependence was observed for **3** in BuCN (Figure 4). Upon lowering the temperature from 293 to 123 K, the intensity increases by more than two orders of magnitude. Drastic changes in intensity are observed in a narrow, low temperature range below 140 K, that is, when butyronitrile becomes glassy (Figure 4D). These changes are accompanied by spectacular blue shifts of the emission: upon lowering the temperature by just five degrees, from 128 to 123 K, the fluorescence maximum shifts from 592 to 544 nm (Figure 4C). Below 123 K, the quantitative measurements are difficult, due to fluctuations of intensity associated with long-term instability of butyronitrile glass. However, it can be safely concluded that both intensity and shape of fluorescence do not change much in the low temperature region. The low temperature emission consists of one band with maximum at 537 nm. This band is barely visible at 293 K, where the fluorescence is dominated by a band with maximum around 650 nm.

The above results demonstrate the influence of viscosity on the photophysics of **3** in a polar solvent, suggesting a conformational change involving a large amplitude motion and a high dipole moment of the excited species.

The temperature dependence of the emission of boranil derivative **3a** in butyronitrile (Figure S3 in the Supporting Information) is similar to that observed for **3**. At room temperature, weak dual fluorescence is observed, with the maxima located at around 490 and 630 nm. The intensity and position of the lower energy band strongly depend on temperature: at 143 K, the intensity increases by a factor of twenty with respect to the value measured at 296 K. Similarly to **3**, the shape of the emission changes dramatically in a narrow temperature range between 138 and 133 K. (Figure S3C). Further decrease of temperature does not lead to significant changes; the fluorescence consists of a single band with a maximum at 487 nm, very close to that of F_1 fluorescence at room temperature.

Comparison of the emission properties of **3** and **3a** indicates that in both molecules the initially excited structure is transformed into a strongly polar transient species that undergoes a viscosity-dependent relaxation process.

Protic solvent solutions

We have also recorded absorption and fluorescence in protic solvents, methanol, and *n*-propanol. While the absorption spectra resemble those obtained in other solvents, the emission profile is quite different. Indeed, multiple bands are observed with relative intensities dependent on the excitation wavelength. This behaviour may have several origins. The first

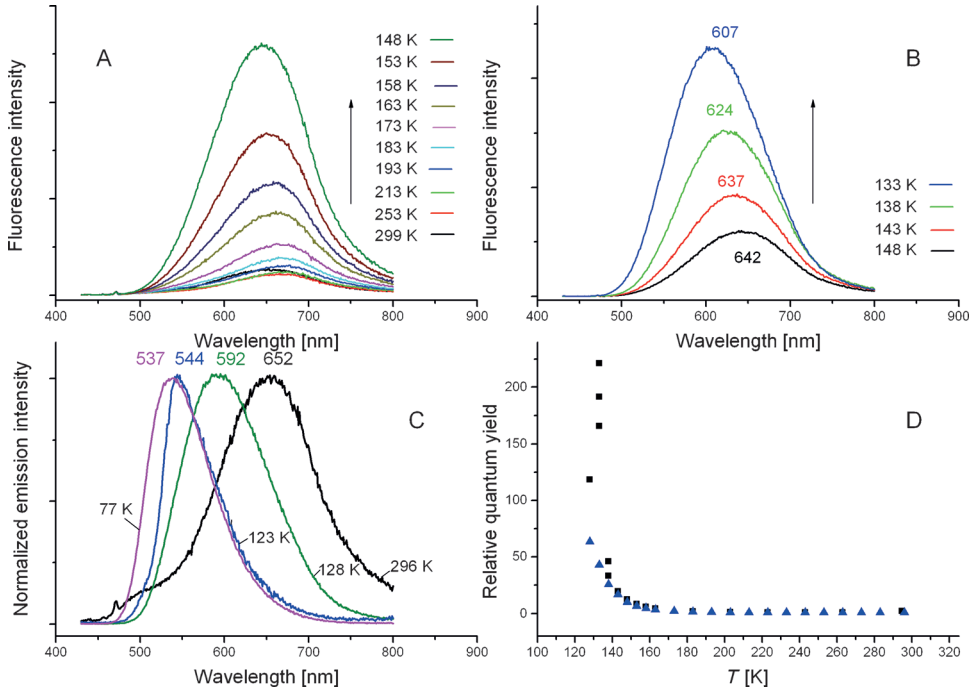

Figure 4. A–B) Temperature dependence of fluorescence of **3** in butyronitrile. C) Fluorescence spectra recorded at 296, 128, 123, and at 77 K. D) Integrated fluorescence intensity relative to the value at 296 K; black and blue symbols indicate measurements on different spectrofluorimeters (Jasny and Edinburgh, respectively).

is trivial for boranils: they can be transformed back to anils by boron decomplexation. Indeed, we have observed that, for instance, **1b** is rapidly converted to **1**. The other source of complicated spectra may be due to the formation of hydrogen-bonded complexes with alcohols. This should, in particular, affect the spectra and photophysics of anils if the alcohol breaks the intramolecular OH···N hydrogen bond. The complex behaviour in alcohols definitely requires further studies.

Kinetic studies

Fluorescence studies

The temporal resolution of our TC-SPC setup, estimated as 20–30 ps, allowed the reliable measurement of the longest components of fluorescence decays (Table 1). Nanosecond decay times are observed in nonpolar environments for the boranils **2a**, **3a**, and **3b**, whereas for **1b** and, in particular, for **1a** the fluorescence decays faster (760 and 120 ps, respectively). In polar solvents, fluorescence lifetimes decrease dramatically with **1b** being the only exception. For the fluoro and cyano derivatives this behaviour correlates well with the corresponding changes in quantum yields, suggesting that the structure responsible for the emission is similar in nonpolar and polar solvents. However, in the nitro anil **3a** the ratio of quantum yields in toluene and acetonitrile is much larger than that of the lifetimes. This indicates a smaller value of the radiative constant in the species emitting in a polar solvent, a hypothesis that was corroborated by time-resolved emission experiments discussed below.

In contrast to the behaviour of boranils, the F_2 decay in the anils **1** and **2** is insensitive or only weakly dependent on the nature of the solvent. This is not the case for the nitro derivative **3**, which exhibits shorter decay in a polar environment.

In order to probe shorter fluorescence decays and to monitor time-resolved spectra, the techniques of fluorescence upconversion (FU) and transient absorption (TA) were used. Exemplary time-wavelength maps obtained using FU are shown in Figure 5, whereas Figure 6 presents the time evolution of fluorescence of **2**, **3**, and **3a**. Table 1 summarizes the decay parameters obtained for all compounds in various solvents. The decays are biexponential, the shorter occurs in the subpicosecond range. The decay time values obtained by fluorescence upconversion correspond well to the kinetic parameters extracted from transient absorption studies.

The components of the dual emission of the anils **1** and **2** reveal a characteristic kinetic pattern. The decay of F_1 fluorescence, occurring in a few hundred femtoseconds to a few picoseconds, is definitely shorter in nonpolar solvents. This finding is in agreement with stationary measurements which show that the F_1/F_2 intensity ratio increases in acetonitrile with respect to toluene (Figures 1 and 2). The F_2 emission decay is much longer and not strongly solvent-dependent, as already noted on the basis of TR-SPC experiments. Time-resolved emission spectra clearly show the ultrafast decay of F_1. In order to check whether the precursor–successor relationship exists between F_1 and F_2, we looked for the rise time in the latter that would correspond to the decay of the former. However, no such rise time could be detected. This result does not exclude the F_1 emitting state as a precursor of F_2, but it may indicate a much lower radiative constant in the latter. Additionally, the rise time may be masked by spectral overlap between the two emission bands.

For **2**, we have also studied the isotope effect. In the OD-deuterated **2**, the F_1 decay time in acetonitrile increases from 2.2 to about 9 ps. Deuteration does not affect the F_2 lifetime. This result strongly suggests that the decay of F_1 is associated with the OH proton translocation. The definitive argument for photoinduced tautomerization was provided by time-resolved IR studies, discussed below.

The kinetic behaviour of **3** is completely different from that observed for the other two anils. Now, both decay components are shorter in acetonitrile. A similar behaviour, a huge

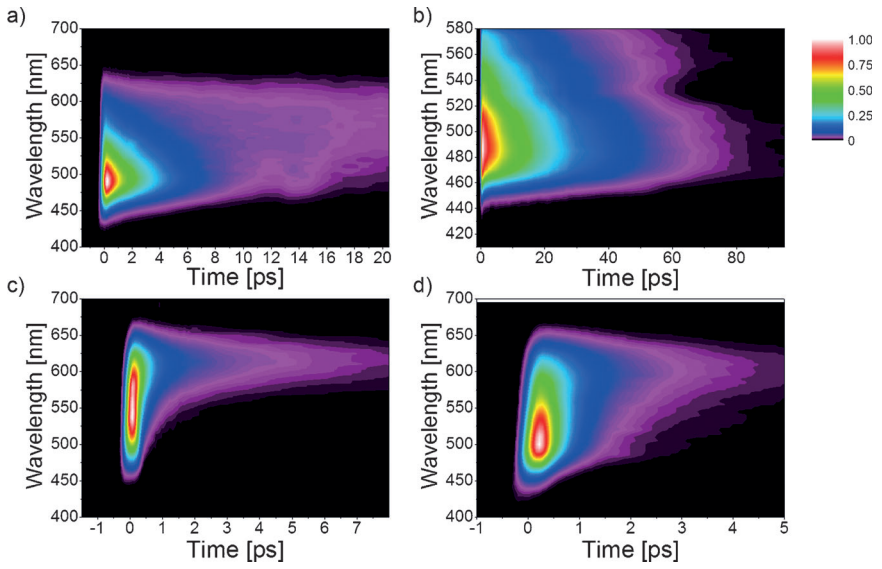

Figure 5. Maps of time-resolved fluorescence of: a) **2**, b) **2a**, c) **3**, and d) **3a**. The spectra were recorded at 293 K using acetonitrile as solvent.

decrease of the decay parameters in polar solvents is observed for **3a** and **3b**.

Inspection of time-resolved emission spectra (Figure 6) clearly shows higher radiative rates for F_1 than for F_2 emissions. This is true both for F_2 occurring from a proton-transferred species and in the case when the origin of the low energy emission must be different (**3a**).

Transient absorption studies

Representative examples of femtosecond transient absorption (TA) spectra are shown in Figures 7, 8, 9, 10. Table 1 contains the decay parameters extracted from the spectra. Other examples of TA, together with decay associated spectra are shown in Figures S4–S9 in the Supporting Information.

The TA spectrum of **2** (Figure 7 and Figure S6 in the Supporting Information) consists of several bands. The negative features at 400 and 500 nm correspond to ground-state bleaching and stimulated F_1 emission, respectively. Due to a much lower radiative constant responsible for F_2, its contribution is not observed in the TA signal. The kinetic profiles measured at 500 nm are in excellent agreement with the fluorescence upconversion results (Table 1). In particular, the F_1 fluorescence decay times, longer in acetonitrile than in toluene, are reproduced.

The transient absorption features a strong peak at 450 nm that overlaps with both bleaching and stimulated fluorescence, so that the kinetic analysis is rather complex. It clearly contains the slower decay component associated with F_2 (209 and 156 ps in toluene and acetonitrile, respectively), but the faster component (0.86/2.5 ps) is also detected. Thus, the TA in this region contains contributions from the species responsible for both F_1 and F_2 emissions.

The time evolution of TA, measured in four solvents may in each case be fitted with three components. The shortest is assigned to the decay of the initially excited species via proton transfer. We note that no recovery of the bleaching is observed on the short time scale. This means that proton transfer does not compete with other fast depopulation channels, which was postulated for SA.[41,42,48] On the contrary, the second component, about 200 ps, assigned to the decay of the phototautomer, appears also at wavelengths corresponding to bleaching, indicating that the rate of ground state back proton transfer is faster than 5×10^9 s^{-1}.

The third decay corresponds to the lifetime which is too long (>15 ns) to be measured accurately with the femtosecond

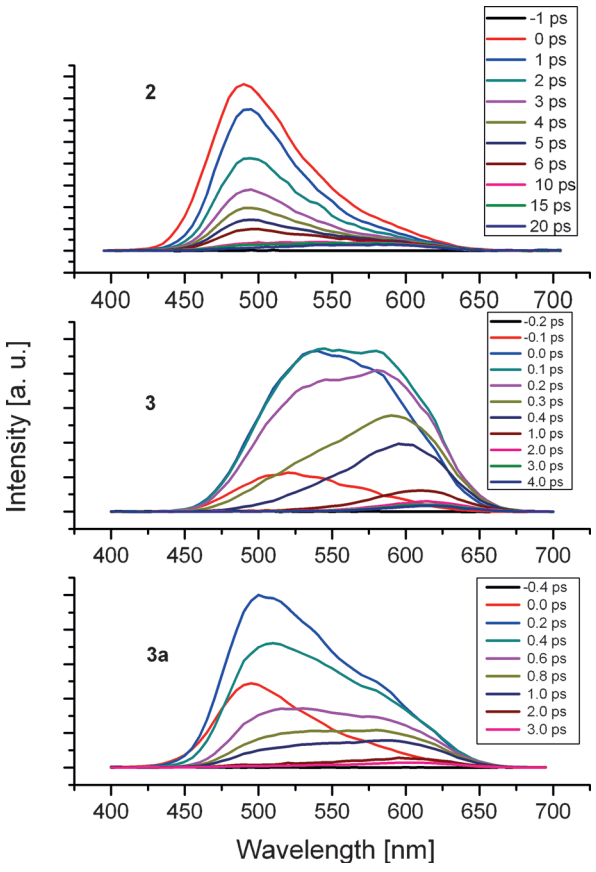

Figure 6. Time-resolved fluorescence spectra of **2**, **3**, and **3a** obtained by FU for acetonitrile solutions at 293 K.

spectrometer. The observation that the TA signal persists after decay of both emissions indicates the presence of a long-lived species. From the magnitude of the bleaching it can be esti-

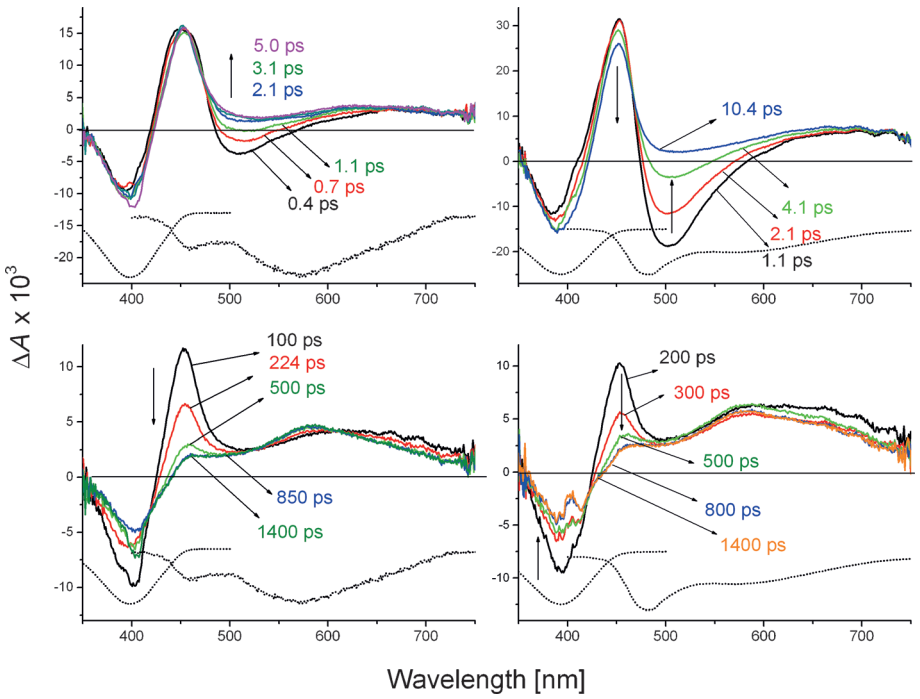

Figure 7. TA of **2** in toluene (left) and acetonitrile (right), recorded at short and long delays (top and bottom, respectively). Dotted lines: inverted stationary absorption and emission.

an ultrafast proton transfer, the molecule has no time to reveal the *cis*-enol fluorescence shift. A significant difference between **2** and **2a** is the lack of any transient signal in acetonitrile at 100 ps delay in **2a**. Thus, contrary to the case of the anil analogue, no long-lived species is now formed. This result suggests that the long-lived transient in **2** is rather due to the photochromic form (*trans*-keto) than to the triplet, since the latter should be also populated in **2a**.

Similar results were obtained for **1** and **1a** (Figures S4–S5 in the Supporting Information). Also in this case, the significant difference between the anil **1** and boranil **1a** is that the former exhibits a long-lived TA signal (peaking at 420 and 530 nm), whereas the latter does not: its decay corresponds to that of fluorescence.

mated that about 50% of the initially excited population does not return to the initial ground state form on the time scale of at least 15 ns. The long-lived species, with the absorption peaks at 460 and 580 nm, may correspond to the photochromic products and/or to the triplet state.

The TA spectra of **2a** (Figure 8 and Figure S7 in the Supporting Information) exhibit a longer component that can be correlated with the decay time of fluorescence. Its value drastically decreases with solvent polarity, in parallel with quantum yield (Table 1). In contrast to the behaviour of **2**, evolution of the transient absorption and stimulated emission signals is observed on the short time scale. The kinetic profiles in this range can be fitted to either mono- or biexponential decay functions. We attribute this evolution to vibrational relaxation and to the stabilization of a large S_1 dipole moment by a polar solvent. The calculations predict a value of 12.6–15.9 D (depending on the method, see Table S1 in the Supporting Information) for the initially excited **2a**. Also for **2**, the S_1 the dipole moment is calculated to be large, but, because of

The TA behaviour of **3** and **3a** is quite complicated (Figures 9 and 10, Figures S8–S9 in the Supporting Information). For **3** in toluene, the strong TA band at 459 nm evolves into a band with a maximum at 481 nm within a few picoseconds. It should be stressed that this evolution corresponds not to a band shift, but to the decay of the high energy feature and

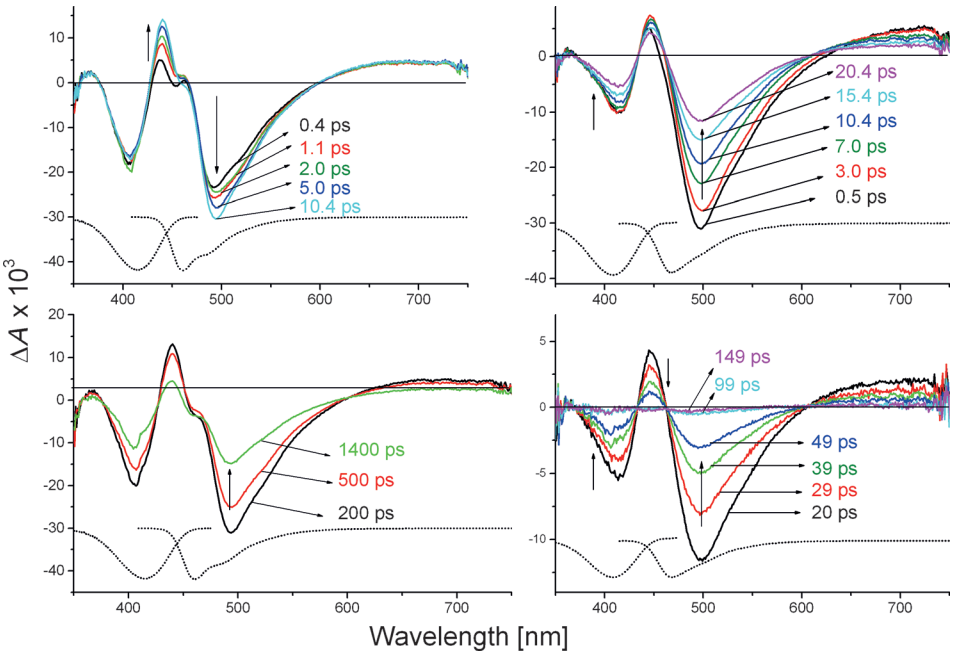

Figure 8. TA of **2a** in toluene (left) and acetonitrile (right), recorded at short and long delays (top and bottom, respectively). Dotted lines: inverted stationary absorption and emission.

formation of the lower energy one. The band at 481 nm and the stimulated emission at 542 nm decay in 260 ps, which is the fluorescence decay time measured by TC-SPC. Interestingly, the intensity of the bleaching signal does not change much during this period. It remains practically constant up to 1300 ps, the longest delay used, during which time, a build-up of TA absorption in the region above 550 nm is observed. An analogous pattern, interconversion of two TA bands, has been observed for ethyl ether, THF, and butyronitrile solutions. The difference with respect to toluene is that a significant time shift of the stimulated emission maximum is now observed, its value reaching 551 nm in diethylether, 579 nm in THF, and 700 nm in butyronitrile. Even a larger shift, to 727 nm, is observed for acetonitrile (Figure 9). In this solvent, only one TA band is observed, shifting from 487 nm, observed immediately after excitation, to 482 nm at longer delays. A shoulder at higher energies is detected at early delays, suggesting that the initially excited species decays in acetonitrile faster than in other solvents. In contrast to anils **1** and **2**, no long-lived transient could be observed for both acetonitrile and butyronitrile solutions.

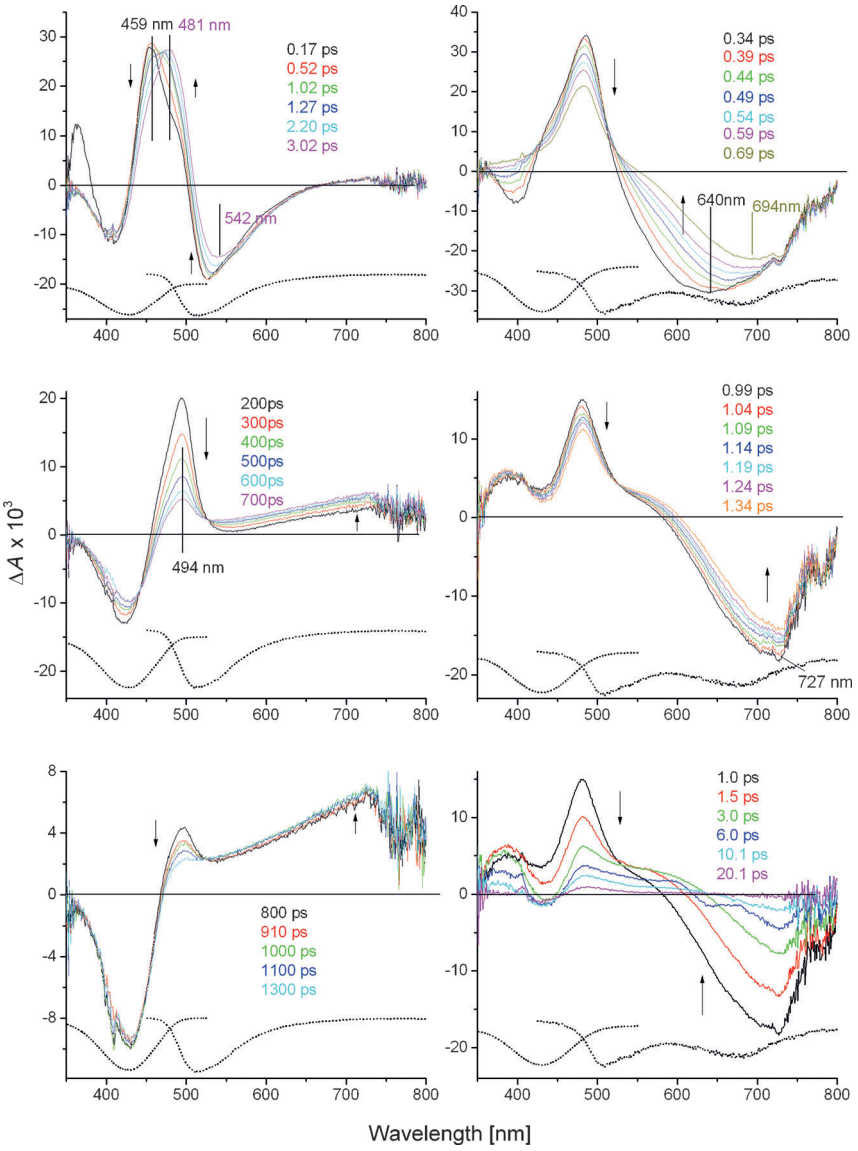

Figure 9. TA of **3** in toluene (left) and acetonitrile (right) for selected time windows. Dotted lines: inverted stationary absorption and emission.

The boranil derivative **3a** (Figure 10 and Figure S9 in the Supporting Information) exhibits a behaviour similar to **3** regarding the temporal evolution of the stimulated emission, but some differences are observed in the region of the TA band. These differences are difficult to quantify because of strong overlap of absorption and fluorescence. Another complication is introduced by very different fluorescence intensities of **3** and **3a** in nonpolar solvents.

The analysis of the strong negative signal due to stimulated fluorescence in acetonitrile yielded the kinetic parameters of 0.6 and 0.7 ps for **3** and **3a**, respectively. These values resemble the relaxation time of acetonitrile,[49] suggesting that the emission initially occurs from a non-relaxed state and that its decay is solvent controlled.

Femtosecond transient IR studies

Figure 11 shows the IR transient spectra of **1** taken after excitation at 400 nm. At short time delays, the transient spectra are dominated by four ground-state bleach bands at 1510, 1585, 1607, and 1635 cm^{-1}, and a positive band at 1545 cm^{-1}. This latter band decays completely within about 150 ps, whereas the bleach bands recover only partially, and new positive bands at about 1500, 1600 and 1640 cm^{-1} appear. From about 150 ps onward, the spectra remain essentially constant up to 1.8 ns, the upper limit of the experimental time-window. Global analysis of the transient IR absorption data was performed using the sum of three exponential functions, and yielded 2.9 ps, 45 ps and >10 ns time constants and the decay-associated spectra shown in Figure S10 in the Supporting Information. The two longest time constants values are in

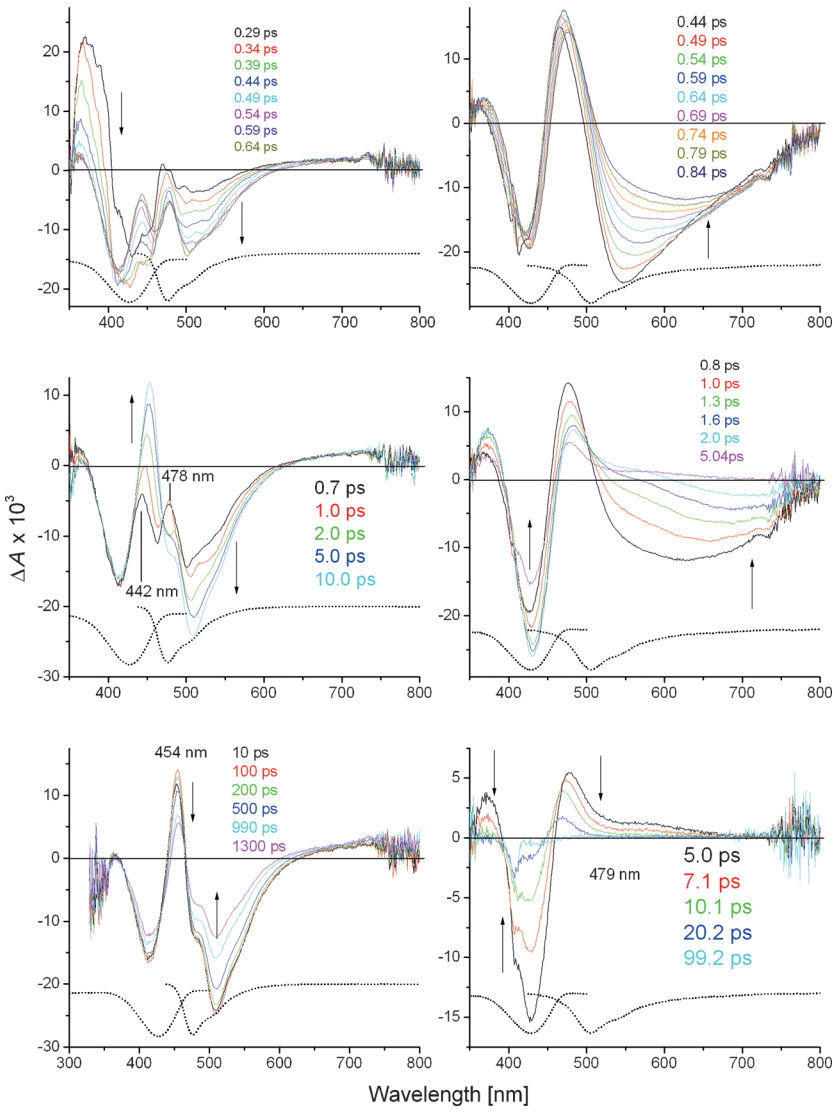

Figure 10. TA of **3a** in toluene (left) and acetonitrile (right) for selected time windows. Dotted lines: inverted stationary absorption and emission.

good agreement with those extracted from the transient visible absorption experiments performed for the same molecule. However, the 2.9 ps lifetime is much longer than that of 0.41–0.45 ps obtained from the FU and transient visible absorption measurements. The transient spectra recorded before 500 fs have not been included in the global analysis of the IR data to avoid the complications related to cross-phase modulation and, thus, this ultrafast component, associated with the ESIPT cannot be detected. To better ascribe the 2.9 ps time constant a global target analysis assuming an A→B→C→D reaction scheme has been carried out. Such analysis yielded the same time constants, as expected, and the species-associated difference spectra shown in Figure S11 in the Supporting Information. The difference spectra associated with A and B are very similar and, therefore, these species can be ascribed to the unrelaxed and relaxed ESIPT product forms of **1**, respectively.

The same measurements were repeated for **2**. The spectra (Figure 12) show three negative bands at 1510, 1570, and 1630 cm^{-1} and positive transient bands at 1530, 1550 and 1595 cm^{-1}, growing within a few picoseconds. In comparison with **1**, where the transient band at 1545 cm^{-1} is present within the time resolution of the experiment, the signal, which is assigned to intramolecular proton transfer, rises more slowly in the cyano derivative **2**. Again, this finding is in good agreement with the results of fluorescence upconversion and transient absorption experiments.

Target analysis using the same scheme as for **1** was performed for **2** (Figure S12 in the Supporting Information), providing a time constant of 4 ps, comparable to 2.2/2.5 ps extracted from fluorescence upconversion and transient-absorption studies. In this case, species A and B can be ascribed to the excited enol and keto forms of **2**, respectively.

Quantum chemical calculations were performed to assign the transient bands observed in the time-resolved IR experiments. Figure 13 shows the comparison of the calculated difference of IR spectra of the keto and enol forms of **1** with the experimental difference spectra. After excitation, positive bands due to the proton transfer are expected. The growth of the

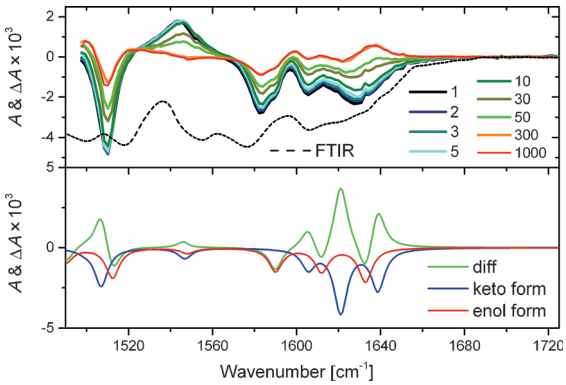

Figure 11. Upper panel: transient IR spectra measured for **1** in acetonitrile at different delays after excitation at 400 nm. The dashed line is the inverted and scaled stationary FTIR spectrum. Lower panel: calculated steady state IR spectra of enol and keto forms (red and blue, respectively) and their difference (green). For a better comparison the calculated spectra were scaled and flipped.

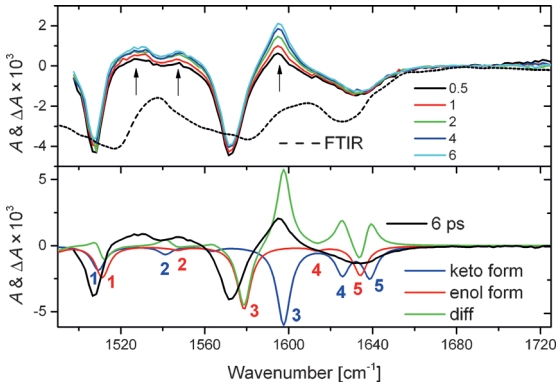

Figure 12. Upper panel: transient IR spectra measured for **2** in acetonitrile at different delays [ps] after excitation at 400 nm. The dashed line is the inverted FTIR spectrum. Lower panel: calculated ground state FTIR spectra for the enol and keto forms (red and blue, respectively), the difference (green), and the experimental spectrum recorded after 6 ps (black). The numbers correspond to the modes depicted in Figure S13 in the Supporting Information.

band at 1600 cm^{-1} in the experimental data coincides with that calculated for the keto form. A positive band is also expected around 1540 cm^{-1}. The modes calculated for **2** in the region between 1500 and 1700 cm^{-1} (Figure S13 in the Supporting Information) involve the OH or NH bending and the C7H and CH bending in the aromatic rings where an influence can be expected when the proton transfer occurs.

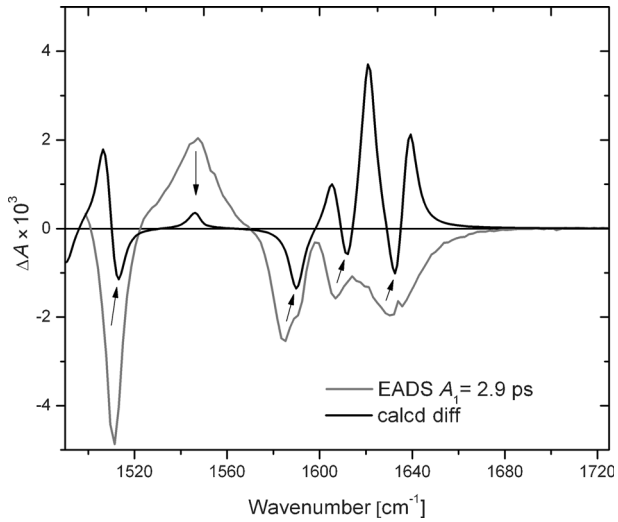

Figure 13. Black: difference of the calculated (B3LYP/6-31 + G(d,p)) steady-state IR spectra for the enol and keto forms of **1**. Grey: evolution associated difference spectra (EADS) of species A obtained from target analysis.

Time-resolved IR measurements were also performed on the nitro substituted anil **3** (Figure S14 in the Supporting Information). All the spectral changes end after a few picoseconds. The decay of the excited state is slightly faster than the recovery of the ground state, probably because of the involvement of a hot ground state, as testified by the positive feature on the low frequency side of the bleach. The intensity of the signals is lower than for the other compounds and the quality of the experimental data did not allow carrying out a target analysis using all the regions.

Calculations

Ground- and excited-state geometry optimizations were carried out in order to determine the structure of the emitting species and the nature of processes responsible for substituent- and solvent-dependent photophysics. To simplify and speed up the calculations, dimethylamino substituent was used instead of diethylamino group. In addition to optimizing the push–pull structures of all the molecules under study, we also computed and analysed the parent molecule, SA, and four model compounds, selected to separately assess the role of electron-donating and -accepting substituents. These included SA singly substituted with the dimethylamino group on the phenol ring (SADMA) and SA with fluorine (SAF), cyano (SACN), and nitro ($SANO_2$) groups on the aniline moiety (Figure S15 in the Supporting Information). The results are presented in Table S1 in the Supporting Information. Three different functionals were tried: 1) B3LYP; 2) PBE0, which is known to yield accurate electronic transition energies, and 3) CAM-B3LYP, recommended for treatment of charge-transfer states.

In general, no significant differences were obtained for ground state optimizations using different functionals. The energies of the lowest singlet electronic transitions were reproduced with similar accuracies by B3LYP and PBE0, whereas using the CAM-B3LYP functional yielded overestimated energies. For this reason, most calculation were done using B3LYP; this also ensured compatibility with previous theoretical studies.[41,42,50] We also checked that double and triple zeta basis sets yielded very similar results, as can be seen from Table S1 in the Supporting Information.

Very similar geometries of the dominant, ground state *cis*-enol form have been obtained for all the analysed molecules. Due to the stabilizing effect of the intramolecular hydrogen bond in anils or boron in boranils, the quasi-six-member ring assumes a nearly planar geometry. On the other hand, considerable twisting about the N1C6 bond is predicted, with the values of the angle α (Scheme 2) in the range of 30–40 degrees. These predictions are in good agreement with the X-ray structure of SA.[51] The calculated ground state dipole moments increase from about 2 D in SA and SAF, to over 3 D in SADMA, and over 5 D in SACN and $SANO_2$. A spectacular push–pull effect, leading to a considerable increase of the dipole moment is observed for both anils and boranils. Calculations systematically yield larger ground state dipole moments for boranils than for the corresponding anils.

As already reported for some boranils,[52] the calculations predict that electronic excitation to S_1 results in the increase of dipole moment. This effect is stronger for anils; no significant change is obtained for boranils **1a** and **1b**. For the cyano derivatives, an almost twofold increase is predicted for the anil **2**, whereas the change in **2a** is smaller (one should note, though, that the S_0 value is larger for the boranil). A spectacular increase is obtained for the nitro derivatives **3** and **3a**, for which the values of nearly 30 D are calculated for the Franck–Condon (FC) geometry corresponding to S_0. Because the dipole moments calculated for the optimized excited *cis*-keto forms are lower, one can expect that the enol form will be stabilized

with respect to the keto species in more polar solvents. We checked the dependence of the S_1 dipole moment in the enol form of **2** on the proton position by increasing the proton in steps of 0.1 Å from the optimized location (OH = 0.998 Å). For the OH distances of 0.998, 1.1, 1.2 1.3, and 1.4 Å the following values of dipole moments were predicted: 16.96, 16.44, 15.41, 14.95, and 15.91 D. In the S_1-optimized *cis*-keto form, the predicted dipole moment is 15.85 D. These result suggest that the barrier to proton transfer should increase in polar environment, in excellent agreement with the experimental results, which reveal slower phototautomerization in acetonitrile than in toluene.

Optimization of the S_1 geometry for model molecules, as well as for **1** was either not convergent or was leading to twisted structures ($\beta \approx 90^\circ$) with energies very close to that of the ground state. This is in agreement with previous findings that showed twisting towards non-planar geometries, corresponding to the regions of S_0/S_1 conical intersection.[20,21,41,42,50,53] However, S_1 geometry could be optimized for other model compounds, anils, and boranils. For **2**, a completely planar structure was found. Also for the boranil derivative **2a** a more planar structure is predicted in S_1, with the angle α decreasing to 17° from 40° in S_0. The predicted Stokes shifts compare satisfactorily with the experiment. These results suggest that upon passing from SA to push–pull substituted anils, the initially excited *cis*-enol form should become more stable with respect to twisting. Comparison of the electronic charges on the oxygen and nitrogen atoms involved in intramolecular H bonds in the S_0, S_1(FC) and optimized S_1 states revealed that the driving force for tautomerization is coupled to the twisting about the C7N1 bond. For **1**, the respective values on the oxygen are −0.32, −0.31. and −0.19; for nitrogen, the calculations yield 0.03, 0.03 and −0.07. The corresponding values for **2** are −0.57, −0.56, and −0.56 (oxygen) and −0.62, −0.59, and −0.62. These results indicate that blocking or slowing down the twisting around C7N1 should lead to a decrease in the excited state proton transfer rate. This prediction is confirmed by the decay times of the initially excited forms: about 50 fs in SA,[31] 250–500 fs in **1**, and 0.8–2.5 ps in **2**.

The different behaviour of the nitro derivatives observed in the experiments was also reproduced by excited state geometry optimizations. In contrast to the planarized geometries of **2** and **2b**, a charge transfer S_1 state with a twisted structure ($\alpha \approx 90^\circ$) was obtained for both **3** and **3a** (and also for the nitro model compound, $SANO_2$). One should note that the twisted form is now characterized by the angle α close to 90 degrees and so it is different from the CI1 and CI2 structures shown in Scheme 2, for which the angles β and γ were involved. The calculated $S_1 \rightarrow S_0$ transition energies are somewhat higher than the positions of the F_2 emission in **3** and **3a**. It should be noted, however, that, because of a huge S_1 dipole moment, the emission in acetonitrile should be strongly red-shifted with respect to the position predicted for an isolated molecule. The origin of charge transfer character is clearly seen upon inspection of molecular orbitals (Figure S16 in the Supporting Information). The S_1 state is represented, both in absorption and emission by a practically (98%) single configuration, involving the electron promotion from a highest occupied molecular orbital (HOMO) to the lowest unoccupied one (LUMO). For the ground state geometry these orbitals are delocalized over the whole molecule, even though the HOMO is preferentially located on the dimethylaniline part, whereas LUMO, on the nitrophenyl moiety. For the twisted S_1 geometry ($\alpha \approx 90^\circ$) HOMO and LUMO become localized on the donor and acceptor parts, respectively. This leads to a TICT (twisted intramolecular charge transfer) state nature of S_1, with the dipole moment approaching 40 D. Actually, the dipole moment is already considerable for the FC geometry of S_1. Its increase upon twisting in **3** and **3a** is opposite to the behaviour predicted for **2** and **2a**, of which the structure becomes more planar in S_1 ($\alpha = 0^\circ$ and 17°, respectively) and the dipole moment decreases.

Table 2 shows the calculated ground- and excited-state values of the lengths of bonds that may be involved in torsional dynamics described by α, β, and γ angles (Scheme 2). We also included the C11N2 bond, to check the possibility of twisting of the diethylamino group. Important differences are obtained for different derivatives, which may explain the photophysical behaviour. Therefore, we discuss these results in detail in the next section.

Table 2. Calculated (B3LYP/6-31G(d,p)) lengths [pm] of the bonds relevant for the torsional dynamics.

		C6N1	C7N1	C7C8	C11N2
SA	S_0	141	128	145	–
	S_1	134	139	142	–
SADMA	S_0	141	130	144	138
	S_1	132	142	139	139
SAF	S_0	141	128	145	–
	S_1	134	139	141	–
SACN	S_0	140	130	145	–
	S_1[a]	139	133	141	–
$SANO_2$	S_0	140	130	144	–
	S_1[a]	147	128	145	–
1	S_0	140	129	144	138
	S_1	132	142	139	139
1a	S_0	143	131	141	137
	S_1	137	139	140	138
2	S_0	140	130	143	137
	S_1	137	132	146	138
2a	S_0	142	132	140	137
	S_1	137	137	141	138
3	S_0	140	130	143	137
	S_1	146	127	148	136
3a	S_0	142	132	140	137
	S_1	147	127	146	137

[a] Values for the S_1 *cis*-keto form, as the optimization converged to this structure.

Discussion

Both experimental and theoretical evidence show that the dual emission, observed for the anils **1** and **2** and absent in their boranil analogues **1a**, **1b**, and **2a** is due to photoinduced proton transfer (ESIPT) from the OH group to the N1 nitrogen atom. FU, TA, and time-resolved IR experiments demonstrate that tautomerization occurs at 293 K in hundreds of femtosec-

onds to a few picoseconds. The reaction is thus much slower than in the parent SA. The rates strongly depend on solvent polarity and the nature of the substituent. The sensitivity to the substituent can be explained by the gradual increase of the barrier to proton transfer in S_1 upon switching from SA to the anils derivatives **1** and **2**. As this barrier reflects the strength of the intramolecular OH···N hydrogen bond, it may be instructive to compare the OH stretching frequencies calculated for different molecules. For the ground state, the calculations for model compounds predict that SA substitution by the dimethylamino group leads to the decrease of this frequency, that is, to a stronger hydrogen bond, whereas, the opposite effect is observed for –F, –CN, and $-NO_2$ substitution. This was also confirmed by the calculated OH stretching frequencies of anils: 3191, 3215, and 3218 cm^{-1} for **1**, **2**, and **3**, respectively. Since the excited-state geometries could not be optimized for all molecules, such systematic comparison was not possible for S_1. However, a huge decrease in the OH frequency calculated for **2** in S_1, to 2794 cm^{-1} can be noted, accompanied by the decrease of the O–N distance from 263 to 258 pm, which shows a drastic increase of driving force for proton transfer.

The lower proton transfer rates in a polar environment can be explained by the preferential stabilization of the excited, more polar *cis*-enol form. We note that the calculated dipole moment values of the excited *cis*-enol are significantly higher than those of *cis*-keto species only for the non-relaxed Franck–Condon geometries, and therefore this conclusion is valid for the fast reaction regime. However, we checked that calculations yield a similar trend, that is, decrease of the S_1 dipole moment upon elongation of the OH bond for both FC and optimized S_1 geometries of *cis*-enol.

The behaviour of **3** can be interpreted in terms of an electron transfer coupled with conformational change and, possibly, proton transfer. The dual pattern of the emission is now observed also for the boranil analogues **3a** and **3b**. Time evolution of the stimulated fluorescence in the TA spectra recorded in solvents of different polarity indicates a large value of the dipole moment of the emitting species. Moreover, huge dependence of the F_2 emission on solvent polarity and viscosity, as revealed by temperature dependence of the emission, points not only to the large dipole moment of the emitting species, but also to large amplitude motion in the relaxation process involved in its creation. We therefore assign the low energy emission to the twisted ($\alpha \approx 90^\circ$) polar structure, calculated for both **3** and **3a**. Since such structure can be achieved without proton transfer, the question is whether the twisting is accompanied by tautomerization in the anil **3**. The experiment provides several arguments in favour of this hypothesis. The first is the observation of somewhat different TA patterns in **3** and **3a**. Also, the time-resolved fluorescence spectra look different for **3** and **3a** at early delays (Figure 6) before they evolve into a low energy band, similar in the two compounds and characterized by a small value of the radiative constant. Finally, it is instructive to compare the radiative rates estimated for the initially excited form. Using the data in Table 1, one obtains for **3a** similar values, $(1–3)\times10^8\ s^{-1}$, for both polar and nonpolar solvents. However, for **3** in toluene, a much lower value is obtained if one uses the value of 260 ps as the fluorescence decay of the excited *cis*-enol form. The discrepancy disappears if the 260 ps decay is associated with the proton-transferred species, for which both FU experiments and calculations predict a lower radiative rate; one should note that, for this reason, the 260 ps component is detected by SPC and TA, but not FU. All these findings indicate that the low energy emission of **3** could correspond to the twisted tautomeric species. Still, we note that the long-lived transient, a characteristic sign of ESIPT, is observed only for toluene solutions of **3**. It may be that the rotation around α slows down the twisting around γ. Another explanation is a much shorter excited state lifetime due to quenching of the S_1 state in polar solvents, which we discuss below.

A spectacular effect is that the fluorescence quantum yields and lifetimes of boranils in solvents with low dielectric constant are higher than those of the corresponding anils, by as much as one or two orders of magnitude. This makes a significant contribution of twisting involving α and β angles in the excited anils rather improbable as major non-radiative depopulation channels, since such processes are allowed for both anils and boranils. On the other hand, this result emphasizes the importance of relaxation which changes the value of γ, because this process is blocked in boranils. Such relaxation is possible in the *cis*-keto forms, and should lead to the photochromic *trans*-keto structure. Indeed, long-lived transients are observed for anils, but not for boranils.

The boranils, devoid of the hydroxyl group, show very strong fluorescence in nonpolar environment, but the quantum yield and lifetime drastically decrease for polar solvents. It seems that the emitting species have the same structure in solvents of different polarity. This is indicated by the values of the radiative constants, practically the same in different solvents: $(4\pm1)\times10^8\ s^{-1}$ for **1a**, $(1.2\pm0.3)\times10^8\ s^{-1}$ for **1b**, and $(3\pm1)\times10^8\ s^{-1}$ for **2a**. The observed fourfold decrease of the radiative constant in **1b** versus **1a** is in excellent agreement with theoretical predictions (Table S1 in the Supporting Information).

The large dependence of fluorescence intensity of boranils on temperature and solvent viscosity in polar environments indicates that the quenching involves a large amplitude motion, most probably twisting. Due to the rigidifying character of BX_2, relaxation involving the angle γ is rather improbable; also the calculations do not predict such a possibility. The calculated C11N2 bond lengths (Scheme 1) remain the same in S_0 and S_1, which rules out the twisting of the diethylamino group. Thus, two angles, α and β have to be taken into account (Scheme 2). Twisting around the C7N1 bond, involving β, is predicted by calculations for SA and SADMA to guide the excited molecule towards the region of CI with the ground state. For twisting involving α, such behaviour is not predicted. We therefore conclude that the quenching channel is related to the increase of β. Since the effect strongly increases with solvent polarity, such twisting most probably involves an electronic state with a large dipole moment. Since no transient intermediate was detected, and the rates of S_1 decay and S_0 repopulation seem to be equal, such a state only provides a doorway to efficient deactivation, but is not populated itself.

In order to understand the role of substituents in the excited state torsional dynamics, we analyse the results of calculations regarding changes of bond lengths upon excitation (Table 2). Practically the same pattern is observed for all the anils and boranils in their ground electronic state. In contrast, the excited-state values of the C6N1 and C7N1 bond lengths, responsible for α and β torsional motions, drastically change with the nature of substituent. For molecules without an electron accepting group (SA, SADMA) or those with a weak acceptor (SAF, **1** and **1a**) the C6N1 and C7N1 bond lengths decrease and increase in S_1, respectively. The opposite is true for the compounds with strong acceptors ($SANO_2$, **3**, **3a**): now the C6N1 bond becomes longer and the C7N1 bond shorter. The cyano-substituted molecules (SACN, **2**, **2a**) are on a borderline between these two patterns, the two bonds being of similar lengths in S_0 and S_1. The influence of the dimethylamino group is rather minor, as can be deduced from the comparison of corresponding pairs (SA vs. SADMA, SAF vs. **1** and **1a**, SACN vs. **2** and **2a**, and $SANO_2$ vs. **3** and **3a**).

It now becomes clear why differently substituted anils and boranils should exhibit different photophysics. Excitation of nitro-substituted chromophores weakens the C6N1 and strengthens the C7N1 bond. Naturally, this facilitates the α torsional relaxation. On the contrary, in molecules without strong electron acceptors, β-relaxation is preferred in the excited state. In chromophores with moderate electron-accepting properties, both types of torsional dynamics should be slowed down. As a result, planar S_1 conformation is more favourable.

Summary

Anils and boranils exhibit photophysical behaviour that is strongly sensitive to both substitution pattern and environment. Dual emission in anils is due to intramolecular excited state proton transfer. Boranils **1a**, **1b**, and **2a**, devoid of proton-transfer functionality, exhibit single fluorescence from a state of which the electronic structure is similar to that of the corresponding anil. On the contrary, in the nitro derivatives, dual emission is observed for both anils and boranils. Its origin is the intramolecular electron transfer accompanied by twisting about the C6N1 bond.

The primary emission of both anils and boranils is quenched in polar solvents. Transient-absorption experiments for boranils indicate that the quenching occurs directly to the ground state, without formation of a "dark", long-lived intermediate. On the other hand, long-lived transient species are detected for anils and can be assigned to *trans*-keto forms.

The investigation of anils and boranil shows the importance of all three angles (α, β, γ in Schemes 1 and 2) relevant for torsional dynamics and, in consequence, rapid excited-state deactivation. Moreover, our study provides examples of chromophores in which efficient channels of excited-state deactivation either reinforce or compete against each other. For instance, photoinduced proton transfer in anils **1** and **2** in nonpolar environments induces rapid radiationless deactivation, most probably through twisting motion. Once the possibility of tautomerization is removed by replacement of the OH proton by BF_2 or BPh_2, the rate of S_1 deactivation is drastically reduced. On the other hand, intramolecular charge transfer accompanied by twisting about C6N1 bond, as in **3** or **3a**, leads to a state of which the lifetime is considerably longer than in the case when rotational dynamics involves C7N1 and C7C8 bonds. In other words, effective relaxation increasing the value of angle α suppresses torsional dynamics involving β and γ.

The complicated photophysics of Schiff bases is the result of many possible processes that can occur with similar rates in the excited molecule: proton transfer, electron transfer, torsional dynamics engaging several bonds, *cis–trans* isomerization. Our results allow suppressing or enhancing these processes by a judicious choice of substituent or solvent. Thus, excited state proton transfer rate can be slowed down by increasing the polarity of the surrounding medium. The intramolecular electron transfer can be enhanced by placing a stronger electron acceptor at C3; in contrast, the role of the donor substituent at C11 seems to be minor. Most important, a general model has been proposed which allows predicting the trends in photophysical changes caused by substitution. It is based on the changes in length of important bonds responsible for torsional dynamics: C6N1, C7N1 and C7C8.

We hope that the present results will contribute to the understanding of intricacies in the photophysics of Schiff bases. Currently, we extend the investigations to structures containing two and three identical proton-transfer functionalities in one chromophore. Finally, one should not overlook the application potential of molecules of which the emission properties are very strongly affected by the environment.

Experimental Section

Synthetic procedures

All reactions were performed under a dry atmosphere of argon. All chemicals were used as received from commercial sources without further purification. Dichloroethane was distilled over P_2O_5 under an argon atmosphere. Thin layer chromatography (TLC) was performed on silica gel or aluminium oxide plates coated with fluorescent indicator. Chromatographic purifications were conducted using 40–63 μm silica gel.

General procedure I

To a solution of aniline B (1 equiv) and *p*-TsOH (trace amounts) in dry ethanol was added aldehyde A (1 equiv). The resulting solution was refluxed overnight. After cooling, the desired anil precipitated. It was then filtered, washed with ethanol, pentane and dried under vacuum.

General procedure II

To a stirred solution of anil (1 equiv) in anhydrous dichloroethane at 85 °C was added $BF_3{\cdot}OEt_2$ (2.5 equiv). A colour change occurred or a precipitate appeared revealing the formation of an intermediate. Then DIEA (2.5 equiv) was added to form the desired boranil. The course of reaction was monitored by TLC analysis. After cooling, the reaction mixture was washed with a saturated solution of $NaHCO_3$ and extracted with dichloromethane. Organic layers were dried over $MgSO_4$ and evaporated under vacuum. The product was

purified by silica gel chromatography and eluted with a mixture of dichloromethane and petroleum ether.

General procedure III

To a solution of anil (1 equiv) in distilled toluene was added BPh_3 (1.5 equiv). The resulting mixture was stirred at 90 °C. The course of reaction was monitored by TLC analysis. After cooling, the solvent was removed under vacuum and the residue was purified by silica gel chromatography eluted with a mixture of dichloromethane and petroleum ether.

Synthesis of 1

General procedure I; yellow powder; yield: 85%. ^{1}H NMR (200 MHz, [D$_6$]acetone): δ = 13.30 (1H, s, OH), 8.61 (1H, s, CH Imine), 7.24 (5H, m, CH Arom), 6.36 (1H, m, CH Arom), 6.13 (1H, s, CH Arom), 3.46 (4H, q, CH_2 NEt_2), 1.19 ppm (6H, t, CH_3 NEt_2); ^{13}C NMR (75 MHz, acetone): δ = 163.2, 162.8, 135.8, 135.1, 123.3, 123.2, 116.8, 116.5, 109.9, 104.7, 98.1, 45.1, 12.9 ppm; elemental analysis calcd (%) for $C_{17}H_{19}N_2OF$: C 71.33, H 6.69, N 9.78; found: C 71.24, H 6.57, N 9.68; EI-MS (*m/z*): 286.1 (100).

Synthesis of 2

General procedure I; yellow crystals; yield: 38%. ^{1}H NMR (300 MHz, $CDCl_3$): δ = 13.25 (1H, s, OH), 8.40 (1H, s, CH Imine), 7.47 (4H, ABsys, J_{AB} = 8.7 Hz, $\nu_0\delta$ = 113.7 Hz, CH Arom), 7.18 (1H, d, ^3J = 8,7 Hz, CH Arom), 6.28 (1H, dd, ^3J = 8.7 Hz, ^4J = 2.4 Hz, CH Arom), 6.19 (1H, d, ^4J = 2.4 Hz, CH Arom), 3.42 (4H, q, ^3J = 7.2 Hz, CH_2 NEt_2), 1.23 ppm (6H, t, ^3J = 7.2 Hz, CH_3 NEt_2); ^{13}C NMR (75 MHz, $CDCl_3$): δ = 164.4, 162.3, 153.2, 152.8, 134.7, 133.6, 121.8, 119.3, 109.1, 108.5, 104.6, 97.8, 44.9, 12.9 ppm; elemental analysis calcd (%) for $C_{18}H_{19}N_3O$: C 73.69, H 6.53, N 14.32; found: C 73.45, H 6.28, N 14.09; EI-MS (*m/z*): 293.1 (100).

Synthesis of 3

General procedure I; red powder; yield: 76%. ^{1}H NMR (200 MHz, $CDCl_3$): δ = 13.23 (1H, s, OH), 8.43 (1H, s, CH Imine), 7.77 (4H, ABsyst, J_{AB} = 8.8 Hz, $\nu_0\delta$ = 189.8 Hz, CH Arom), 7.18 (1H, d, J = 8.8 Hz, CH Arom), 6.28 (1H, dd, J_1 = 8.8 Hz, J_2 = 1.9 Hz, CH Arom), 6.19 (1H, d, J = 1.9 Hz, CH Arom), 3.42 (4H, q, J = 6,8 Hz, CH_2 NEt_2), 1.20 ppm (6H, t, J = 6,8 Hz, CH_3 NEt_2); ^{13}C NMR (75 MHz, $CDCl_3$): δ = 164.3, 162.3, 154.8, 152.8, 144.9, 134.7, 125.2, 121.3, 109.0, 104.6, 97.5, 44.8, 12.7 ppm; elemental analysis calcd (%) for $C_{17}H_{19}N_3O_3$: C 65.16, H 6.11, N 13.41; found: C 64.82, H 5.82, N 13.19; EI-MS (*m/z*): 313.1 (100).

Synthesis of 1a

General procedure II; yellow powder; yield: 43%. ^{1}H NMR (200 MHz, [D$_6$]acetone): δ = 8.49 (1H, s, CH Imine), 7.62 (2H, m, CH Arom), 7.47 (1H, d, J = 9.2 Hz, CH Arom), 7.25 (2H, m, CH Arom), 6.55 (1H, dd, J_1 = 9.2 Hz, J_2 = 2.4 Hz, CH Arom), 6.16 (1H, d, J = 2.4 Hz, CH Arom), 3.57 (4H, q, J = 7,2 Hz, CH_2 NEt_2), 1.24 ppm (6H, t, J = 7,2 Hz, CH_3 NEt_2); ^{13}C NMR (75 MHz, $CDCl_3$): δ = 160.6, 157.3, 135.5, 126.1, 126.0, 116.8, 116.5, 107.5, 98.1, 45.6, 12.9 ppm; ^{11}B NMR (128 MHz, [D$_6$]acetone): δ = 0.85 ppm (t, J = 16.7 MHz, BF_2); elemental analysis calcd (%) for $C_{17}H_{18}BF_3N_2O$: C 61.11, H 5.43, N 8.38; found: C 60.84, H 5.19, N 8.33; EI-MS (*m/z*): 334.1 (100), 285.1 (30).

Synthesis of 1b

General procedure III; yellow powder; yield: 78%. ^{1}H NMR (200 MHz, [D$_6$]acetone): δ = 8.44 (1H, s, CH Imine), 7.35 (5H, m, CH Arom), 7.12 (8H, m, CH Arom), 6.94 (2H, m, CH Arom), 6.32 (1H, dd, CH, J_1 = 8.8 Hz, J_2 = 2.2 Hz, CH Arom), 6.02 (1H, d, CH, J = 2.2 Hz, CH Arom), 3.47 (4H, q, J = 6,9 Hz, CH_2 NEt_2), 1.17 ppm (6H, t, J = 6,9 Hz, CH_3 NEt_2); ^{13}C NMR (100 MHz, [D$_6$]acetone): δ = 164.3, 159.9, 156.2, 143.0, 134.7, 133.7, 126.5, 126.4, 126.3, 125.6, 115.0, 114.7, 109.6, 105.2, 97.8, 44.5, 12.1 ppm; ^{11}B NMR (128 MHz, [D$_6$]acetone): δ = 5.17 ppm (s, BPh_2); elemental analysis calcd (%) for $C_{29}H_{28}BFN_2O$: C 77.34, H 6.27, N 6.22; found: C 77.04, H 5.90, N 5.94; EI-MS (*m/z*): 450.1 (100).

Synthesis of 2a

General procedure II; yellow powder; yield: 84%. ^{1}H NMR (200 MHz, $CDCl_3$): δ = 8.05 (1H, br s, CH Imine), 7.67 (4H, ABsys, J_{AB} = 8.8 Hz, $\nu_0\delta$ = 20.0 Hz, CH Arom), 7.24 (1H, d, ^3J = 8.8 Hz, CH Arom), 6.40 (1H, dd, ^3J = 8.8 Hz, ^4J = 2.4 Hz, CH Arom), 6.23 (1H, d, ^4J = 2.4 Hz, CH Arom), 3.48 (4H, q, ^3J = 6,8 Hz, CH_2 NEt_2), 1.26 ppm (6H, t, ^3J = 6,8 Hz, CH_3 NEt_2); ^{13}C NMR (75 MHz, [D$_6$]acetone): δ = 163.4, 160.2, 158.1, 148.1, 136.1, 134.2, 124.8, 119.1, 111.2, 108.4, 98.0, 45.9, 13.0 ppm; ^{11}B NMR (128 MHz, [D$_6$]acetone): δ = 0.90 ppm (t, J = 16.6 MHz, BF_2); elemental analysis calcd (%) for $C_{18}H_{18}BF_2N_3O$: C 63.37, H 5.32, N 12.32; found: C 63.18, H 5.17, N 12.09; EI-MS (*m/z*): 341.1 (100), 322.1 (35).

Synthesis of 3a

General procedure II; orange powder; yield: 72%. ^{1}H NMR (200 MHz, [D$_6$]acetone): δ = 8.67 (1H, s, CH Imine), 8.13 (4H, ABsyst, J_{AB} = 9.1 Hz, $\nu_0\delta$ = 99.4 Hz), 7.52 (1H, d, CH Arom), 6.63 (1H, dd, J = 9.1 Hz, CH Arom), 6.19 (1H, d, CH, J_1 = 9.1 Hz, J_2 = 2.4 Hz, CH Arom), 3.62 (4H, q, J = 7.3 Hz, CH_2 NEt_2), 1.27 ppm (6H, t, J = 7.3 Hz, CH_3 NEt_2); ^{13}C NMR (75 MHz, [D$_6$]acetone): δ = 162.5, 157.3, 157.2, 146.2, 134.6, 125.0, 123.5, 107.7, 98.0, 45.4, 12.7 ppm; ^{11}B NMR (128 MHz, [D$_6$]acetone): δ = 0.88 ppm (t, J = 16.7 Hz, BF_2); elemental analysis calcd (%) for $C_{17}H_{18}BF_2N_3O_3$: C 56.54, H 5.02, N 11.64; found: C 56.32, H 4.72, N 11.42; EI-MS (*m/z*): 361.1 (100), 313.1 (25).

Synthesis of 3b

General procedure III; yellow orange powder; yield: 85%. ^{1}H NMR (200 MHz, [D$_6$]acetone): δ = 8.65 (1H, s, CH Imine), 8.05 (2H, m, CH Arom), 7.30 (7H, m, CH Arom), 7.17 (6H, m, CH Arom), 6.38 (1H, dd, CH, J_1 = 8.8 Hz, J_2 = 2.2 Hz, CH Arom), 6.02 (1H, d, CH, J = 2.2 Hz, CH Arom), 3.47 (4H, q, J = 7,3 Hz, CH_2 NEt_2), 1.17 ppm (6H, t, J = 7,3 Hz, CH_3 NEt_2); ^{13}C NMR (75 MHz, acetone): δ = 165.9, 160.5, 158.0, 152.7, 136.3, 135.0, 134.7, 131.1, 128.3, 127.5, 126.7, 125.9, 124.6, 111.2, 107.1, 98.6, 45.6, 13.0 ppm; ^{11}B NMR (128 MHz, acetone): δ = 5.59 ppm (s, BPh_2); elemental analysis calcd (%) for $C_{29}H_{28}BN_3O_3$: C 72.97, H 5.91, N 8.80; found: C 72.74, H 5.77, N 8.62; EI-MS (*m/z*): 477.1 (100).

NMR characterization

The 300 (^{1}H), 400 (^{1}H), 75 (^{13}C), 100 (^{13}C) 128 (^{11}B) MHz NMR spectra were recorded at room temperature with perdeuterated solvents with residual protonated solvent signals as internal references. The 128 (^{11}B) MHz NMR spectra were recorded at room temperature with borosilicate glass as reference.

Spectral measurements

The spectral grade solvents used for spectral measurements: cyclohexane, tetrahydrofuran, diethyl ether, methanol, *n*-propanol, valeronitrile, butyronitrile, acetonitrile (Merck), and toluene (Roth) were checked for the presence of fluorescing impurities. Butyronitrile was distilled just prior to experiments.

Electronic absorption spectra were recorded on a Shimadzu UV 3100 spectrophotometer. Stationary luminescence spectra were obtained using an Edinburgh FS900 CDT, Jasny[54] or compact Jasny[55] spectrofluorimeters, equipped with sample temperature control systems.

Transient absorption spectra were recorded using a setup based on 1 kHz amplified Ti:Saphire system (Spectra-Physics) as described in detail elsewhere.[56,57] The second harmonic ($\lambda = 400$ nm) was used to excite the sample. The energy per pulse at the sample was around 1 μJ. A white-light continuum generated by focusing pulses at 800 nm into a CaF_2 plate was used for probing. The polarization of the probe beam was at the magic angle relative to that of the pump pulses. All spectra were corrected for the chirp of the probe pulses. The full width at half maximum of the instrument response function was around 200 fs.

Time-resolved fluorescence spectra were measured using femtosecond up-conversion setup, consisting of femtosecond oscillator followed by a home-built regenerative amplifier.[58] The amplified beam was split into two parts: one was used to generate second harmonic beam at 400 nm, while the rest of the beam was used to drive a noncollinear optical parametric amplifier. Second harmonic beam was used for excitation of a sample enclosed in a 200 μm thick quartz cuvette. The fluorescence was then collected by an all-reflective Schwarzschild objective, and then imaged onto the surface of a BBO nonlinear crystal. The fluorescence was temporally gated by an IR beam (1020 nm) generated by a parametric amplifier. The BBO crystal was wobbling, which allowed gating the fluorescence beam in a broad spectral range at once. Such upconverted spectrum was then imaged onto an input slit of a spectrometer. Time-resolved spectra (uncorrected for spectral sensitivity) were measured for different time delays between excitation and gating pulses, which was controlled by the use of a translation stage. The temporal resolution was 150 fs, which was mostly determined by the duration of the excitation pulse. The time constants of the measured fluorescence maps were retrieved using global analysis, as described elsewhere.[59]

Time-correlated single photon counting (TC-SPC) measurements were carried out using a home-built setup. The excitation was provided by a PicoQuant LDH-D-C-375 laser, emitting at 379 nm, with pulse width of about 60 ps and pulse energy in the range of 30–50 pJ. The emission, after passing through a Digikröm CM112 double grating monochromator working in a subtractive mode, was detected by an HPM-100-40 hybrid detector (Becker & Hickl) coupled to a Becker & Hickl SPC-830 TR-SPC module. The decay profiles were analysed using commercially available packages: Fluofit version 3.3 (Picoquant) and FAST version 3.3 (Edinburgh Instruments).

Femtosecond transient IR spectra were recorded upon 400 nm excitation using the pump-probe set up described elsewhere,[60,61] in three different probe windows, from 1500 to 1730 cm^{-1}. The spectra were scaled and merged using the corresponding factor calculated for the first window recorded. Further windows until 1980 cm^{-1} were checked, but no transient signal was present. At least six measurements were recorded in each window and averaged.

Stationary FTIR spectra were recorded on a Perkin–Elmer Spectrum One FT-IR spectrometer (ATR, Golden Gate), with solid samples.

Calculations

The calculations of electronic and vibrational structure in the ground electronic state were performed using density functional theory (DFT). For excited state geometry optimization and for the calculation of electronic transition energies, time-dependent DFT model was applied. Two software packages were used, Gaussian 09[62] and ADF.[63–65]

Acknowledgements

This work has been financed by the funds from the Polish National Science Centre (DEC-2011/01/B/ST4/01130 and 2011/01/B/ST2/02053). We acknowledge a computing grant from the Interdisciplinary Centre for Mathematical and Computational Modeling. This research was also supported in part by PL-Grid Infrastructure. We acknowledge the CNRS and ECPM for providing research facilities and financial support (MRT fellowship for D.F.). J.D. thanks NanOtechnology, Biomaterials and aLternative Energy Source for the ERA Integration project from the European Union (FP7-REGPOT-CT-2011-285949-NOBLESSE). Support from the Swiss National Foundation (Nr. 200020-147098) and the University of Geneva is also acknowledged.

Keywords: anils · boranils · photochemistry · photophysics · ultrafast spectroscopy

[1] M. H. V. Huynh, T. J. Meyer, *Chem. Rev.* **2007**, *107*, 5004–5064.
[2] S. Hammes-Schiffer, *Acc. Chem. Res.* **2009**, *42*, 1881–1889.
[3] C.-C. Hsieh, C.-M. Jiang, P.-T. Chou, *Acc. Chem. Res.* **2010**, *43*, 1364–1374.
[4] H. Petek, J. Zhao, *Chem. Rev.* **2010**, *110*, 7082–7099.
[5] M. Barroso, L. G. Arnaut, S. J. Formosinho, *RSC Catal. Ser.* **2012**, *8*, 126–151.
[6] D. R. Weinberg, C. J. Gagliardi, J. F. Hull, C. F. Murphy, C. A. Kent, B. C. Westlake, A. Paul, D. H. Ess, D. G. McCafferty, T. J. Meyer, *Chem. Rev.* **2012**, *112*, 4016–4093.
[7] O. S. Wenger, *Acc. Chem. Res.* **2013**, *46*, 1517–1526.
[8] J. Bonin, M. Robert, *Photochem. Photobiol.* **2011**, *87*, 1190–1203.
[9] Z. R. Grabowski, K. Rotkiewicz, W. Rettig, *Chem. Rev.* **2003**, *103*, 3899–4031.
[10] T. Scherer, I. H. M. van Stokkum, A. M. Brouwer, J. W. Verhoeven, *J. Phys. Chem.* **1994**, *98*, 10539–10549.
[11] W. Rettig, M. Maus, in *Conformational Changes Accompanying Intramolecular Excited State Electron Transfer* (Ed.: J. Waluk), Wiley-VCH, Weinheim, **2000**, pp. 1–55.
[12] Z. R. Grabowski, *Pure Appl. Chem.* **1992**, *64*, 1249–1255.
[13] J. Herbich, B. Brutschy, in *TICT Molecules, Vol. 4* (Ed.: V. Balzani), Wiley-VCH, Weinheim, **2001**, pp. 697–741.
[14] E. Nosenko, G. Wiosna-Sałyga, M. Kunitski, I. Petkova, A. Singh, W. J. Buma, R. P. Thummel, J. Waluk, *Angew. Chem. Int. Ed.* **2008**, *47*, 6037–6040; *Angew. Chem.* **2008**, *120*, 6126–6129.
[15] E. Hadjoudis, I. M. Mavridis, *Chem. Soc. Rev.* **2004**, *33*, 579–588.
[16] E. Hadjoudis, S. D. Chatziefthimiou, I. M. Mavridis, *Curr. Org. Chem.* **2009**, *13*, 269–286.
[17] R. S. Becker, C. Lenoble, A. Zein, *J. Phys. Chem.* **1987**, *91*, 3517–3524.
[18] R. S. Becker, C. Lenoble, A. Zein, *J. Phys. Chem.* **1987**, *91*, 3509–3517.
[19] V. C. Vargas, *J. Phys. Chem. A* **2004**, *108*, 281–288.
[20] M. I. Knyazhansky, N. I. Makarova, A. V. Metelitsa, A. I. Shif, V. P. Pichko, E. P. Ivakhnenko, *Mol. Cryst. Liq. Cryst. Sci. Technol. Sect. A* **1997**, *298*, 391–396.

[21] M. I. Knyazhansky, A. V. Metelitsa, A. J. Bushkov, S. M. Aldoshin, *J. Photochem. Photobiol. A* **1996**, *97*, 121 – 126.
[22] K. Kownacki, L. Kaczmarek, A. Grabowska, *Chem. Phys. Lett.* **1993**, *210*, 373 – 379.
[23] A. Grabowska, K. Kownacki, L. Kaczmarek, *J. Lumin.* **1994**, *60 – 61*, 886 – 890.
[24] K. Kownacki, A. Mordzinski, R. Wilbrandt, A. Grabowska, *Chem. Phys. Lett.* **1994**, *227*, 270 – 276.
[25] A. Mordziński, K. Kownacki, R. Wilbrandt, C. Rios, *J. Inf. Rec. Mater.* **1994**, *21*, 601 – 604.
[26] A. Grabowska, K. Kownacki, J. Karpiuk, S. Dobrin, L. Kaczmarek, *Chem. Phys. Lett.* **1997**, *267*, 132 – 140.
[27] A. Grabowska, K. Kownacki, L. Karczmarek, *Acta Phys. Pol. A* **1995**, *88*, 1081 – 1088.
[28] C. Okabe, T. Nakabayashi, Y. Inokuchi, N. Nishi, H. Sekiya, *J. Chem. Phys.* **2004**, *121*, 9436 – 9442.
[29] N. Otsubo, C. Okabe, H. Mori, K. Sakota, K. Amimoto, T. Kawato, H. Sekiya, *J. Photochem. Photobiol. A* **2002**, *154*, 33 – 39.
[30] W. M. F. Fabian, L. Antonov, D. Nedeltcheva, F. S. Kamounah, P. J. Taylor, *J. Phys. Chem. A* **2004**, *108*, 7603 – 7612.
[31] M. Ziółek, J. Kubicki, A. Maciejewski, R. Naskręcki, A. Grabowska, *Phys. Chem. Chem. Phys.* **2004**, *6*, 4682 – 4689.
[32] M. Ziółek, J. Kubicki, A. Maciejewski, R. Naskręcki, A. Grabowska, *J. Chem. Phys.* **2006**, *124*, 124518.
[33] M. Ziółek, J. Kubicki, A. Maciejewski, R. Naskręcki, W. Łuniewski, A. Grabowska, *J. Photochem. Photobiol. A* **2006**, *180*, 101 – 108.
[34] M. Ziółek, K. Filipczak, A. Maciejewski, *Chem. Phys. Lett.* **2008**, *464*, 181 – 186.
[35] M. Ziółek, G. Burdziński, K. Filipczak, J. Karolczak, A. Maciejewski, *Phys. Chem. Chem. Phys.* **2008**, *10*, 1304 – 1318.
[36] M. Ziółek, G. Burdziński, J. Karolczak, *J. Phys. Chem. A* **2009**, *113*, 2854 – 2864.
[37] M. Ziółek, M. Gil, J. A. Organero, A. Douhal, *Phys. Chem. Chem. Phys.* **2010**, *12*, 2107 – 2115.
[38] M. Ziółek, C. Martin, M. T. Navarro, H. Garcia, A. Douhal, *J. Phys. Chem. C* **2011**, *115*, 8858 – 8867.
[39] M. Ziółek, G. Burdziński, A. Douhal, *Photochem. Photobiol. Sci.* **2012**, *11*, 1389 – 1400.
[40] M. Ziółek, B. Cohen, X. Yang, L. Sun, M. Paulose, O. K. Varghese, C. A. Grimes, A. Douhal, *Phys. Chem. Chem. Phys.* **2012**, *14*, 2816 – 2831.
[41] T. Sekikawa, O. Schalk, G. Wu, A. E. Boguslavskiy, A. Stolow, *J. Phys. Chem. A* **2013**, *117*, 2971 – 2979.
[42] L. Spörkel, G. Cui, W. Thiel, *J. Phys. Chem. A* **2013**, *117*, 4574 – 4583.
[43] M. H. Luo, H. Y. Tsai, H. Y. Lin, S. K. Fang, K. Y. Chen, *Chin. Chem. Lett.* **2012**, *23*, 1279 – 1282.
[44] T.-C. Fang, H.-Y. Tsai, M.-H. Luo, C.-W. Chang, K.-Y. Chen, *Chin. Chem. Lett.* **2013**, *24*, 145 – 148.
[45] E. Hadjoudis, *Mol. Eng.* **1995**, *5*, 301 – 337.
[46] D. Frath, S. Azizi, G. Ulrich, P. Retailleau, R. Ziessel, *Org. Lett.* **2011**, *13*, 3414 – 3417.
[47] D. Frath, S. Azizi, G. Ulrich, R. Ziessel, *Org. Lett.* **2012**, *14*, 4774 – 4777.
[48] T. Sekikawa, O. Schalk, G. Wu, A. E. Boguslavskiy, A. Stolow, *Springer Proc. Phys.* **2012**, *125*, 313 – 315.
[49] M. L. Horng, J. A. Gardecki, A. Papazyan, M. Maroncelli, *J. Phys. Chem.* **1995**, *99*, 17311 – 17337.
[50] J. M. Ortiz-S ánchez, R. Gelabert, M. Moreno, J. M. Lluch, *J. Chem. Phys.* **2008**, 129, 214308.
[51] R. Destro, A. Gavezzotti, M. Simonetta, *Acta Crystallogr. Sect. B* **1978**, *34*, 2867 – 2869.
[52] S. Chibani, A. Charaf-Eddin, B. Le Guennic, D. Jacquemin, *J. Chem. Theory Comput.* **2013**, *9*, 3127 – 3135.
[53] J. M. Ortiz-S ánchez, D. Bucher, L. C. T. Pierce, P. R. L. Markwick, J. A. McCammon, *J. Chem. Theory Comput.* **2012**, 8, 2752 – 2761.
[54] J. Jasny, *J. Lumin.* **1978**, *17*, 149 – 173.
[55] J. Jasny, J. Waluk, *Rev. Sci. Instrum.* **1998**, *69*, 2242.
[56] G. Duvanel, N. Banerji, E. Vauthey, *J. Phys. Chem. A* **2007**, *111*, 5361 – 5369.
[57] N. Banerji, G. Duvanel, A. Perez-Velasco, S. Maity, N. Sakai, S. Matile, E. Vauthey, *J. Phys. Chem. A* **2009**, *113*, 8202 – 8212.
[58] B. Białkowski, Y. Stepanenko, M. Nejbauer, C. Radzewicz, J. Waluk, *J. Photochem. Photobiol. A* **2012**, *234*, 100 – 106.
[59] P. Fita, E. Luzina, T. Dziembowska, C. Radzewicz, A. Grabowska, *J. Chem. Phys.* **2006**, *125*, 184508.
[60] M. Koch, A. Rosspeintner, K. Adamczyk, B. Lang, J. Dreyer, E. T. J. Nibbering, E. Vauthey, *J. Am. Chem. Soc.* **2013**, *135*, 9843 – 9848.
[61] M. Koch, R. Letrun, E. Vauthey, *J. Am. Chem. Soc.* **2014**, *136*, 4066 – 4074.
[62] Gaussian 09, Revision B.01, M. J. Frisch, G. W. Trucks, H. B. Schlegel, G. E. Scuseria, M. A. Robb, J. R. Cheeseman, G. Scalmani, V. Barone, B. Mennucci, G. A. Petersson, H. Nakatsuji, M. Caricato, X. Li, H. P. Hratchian, A. F. Izmaylov, J. Bloino, G. Zheng, J. L. Sonnenberg, M. Hada, M. Ehara, K. Toyota, R. Fukuda, J. Hasegawa, M. Ishida, T. Nakajima, Y. Honda, O. Kitao, H. Nakai, T. Vreven, J. A. Montgomery, Jr., J. E. Peralta, F. Ogliaro, M. Bearpark, J. J. Heyd, E. Brothers, K. N. Kudin, V. N. Staroverov, T. Keith, R. Kobayashi, J. Normand, K. Raghavachari, A. Rendell, J. C. Burant, S. S. Iyengar, J. Tomasi, M. Cossi, N. Rega, J. M. Millam, M. Klene, J. E. Knox, J. B. Cross, V. Bakken, C. Adamo, J. Jaramillo, R. Gomperts, R. E. Stratmann, O. Yazyev, A. J. Austin, R. Cammi, C. Pomelli, J. W. Ochterski, R. L. Martin, K. Morokuma, V. G. Zakrzewski, G. A. Voth, P. Salvador, J. J. Dannenberg, S. Dapprich, A. D. Daniels, O. Farkas, J. B. Foresman, J. V. Ortiz, J. Cioslowski, D. J. Fox, Gaussian, Inc., Wallingford CT, **2010**.
[63] C. Fonseca Guerra, J. Snijders, G. te Velde, E. Baerends, *Theor. Chem. Acc.* **1998**, *99*, 391 – 403.
[64] G. te Velde, F. Bickelhaupt, S. van Gisbergen, C. Fonseca Guerra, E. Baerends, J. Snijders, T. Ziegler, *J. Comput. Chem.* **2001**, *22*, 931.
[65] ADF2013, SCM, Theoretical Chemistry, Vrije Universiteit, Amsterdam, The Netherlands, http://www.scm.com.

Received: July 31, 2014
Published online on November 20, 2014